

## Original article

# Effects of impurity gases on interfaces of the hydrogen-water-decane three-phase system: A square gradient theory investigation

Yafan Yang<sup>1</sup>✉\*, Jingyu Wan<sup>1</sup>, Jingfa Li<sup>2</sup>, Weiwei Zhu<sup>3</sup>, Guangsi Zhao<sup>1</sup>, Xiangyu Shang<sup>1</sup>✉\*

<sup>1</sup>State Key Laboratory for Geomechanics and Deep Underground Engineering, China University of Mining and Technology, Xuzhou 221116, P. R. China

<sup>2</sup>School of Mechanical Engineering and Hydrogen Energy Research Center, Beijing Institute of Petrochemical Technology, Beijing 102617, P. R. China

<sup>3</sup>Department of Engineering Mechanics, Tsinghua University, Beijing 100084, P. R. China

### Keywords:

Underground hydrogen storage  
cushion gases  
three-phase fluid  
interfacial tension  
square gradient theory

### Cited as:

Yang, Y., Wan, J., Li, J., Zhu, W., Zhao, G., Shang, X. Effects of impurity gases on interfaces of the hydrogen-water-decane three-phase system: A square gradient theory investigation. *Capillarity*, 2023, 9(1): 9-24. <https://doi.org/10.46690/capi.2023.10.02>

### Abstract:

The effects of impurity gases on interfacial characteristics of hydrogen-water-oil three-phase systems are critical to underground H<sub>2</sub> storage in depleted oil fields but have not been investigated yet. The square gradient theory calculations with Perturbed-chain statistical associating fluid theory equation of state are carried out to understand the effects of impurity gases (N<sub>2</sub>, CH<sub>4</sub>, and CO<sub>2</sub>) on interfaces of the H<sub>2</sub>-H<sub>2</sub>O-n-decane three-phase system under reservoir conditions. Our results obtained from the four-component three-phase systems are compared to the corresponding system without impurity gases. It is found that the all three interfaces (H<sub>2</sub>-H<sub>2</sub>O, H<sub>2</sub>O-C<sub>10</sub>H<sub>22</sub>, and H<sub>2</sub>-C<sub>10</sub>H<sub>22</sub>) are greatly influenced by impurity gases. The impurity gases accumulate in all three interfacial regions and have positive surface excesses, which leads to smaller interfacial tensions. The reduction of interfacial tensions depends on the type of impurity gas following this order: CO<sub>2</sub> ≥ CH<sub>4</sub> > N<sub>2</sub>. In general, the adsorption of impurity gases weakens the adsorption of other species. However, the adsorption of decane in the H<sub>2</sub>-H<sub>2</sub>O interface can be enhanced by impurity gases, which also contributes to the decrease of interfacial tensions. Moreover, the spreading coefficients are mostly negative over the studied temperature and pressure conditions indicating the existence of three-phase contact in the N<sub>2</sub>/CH<sub>4</sub>/CO<sub>2</sub>-hydrogen-water-oil three-phase systems.

## 1. Introduction

Currently, the predominant source of energy utilized worldwide is from fossil fuels, including coal, petroleum, and natural gas (Shafiee and Topal, 2009; Abas et al., 2015). The carbon emissions resulting from the combustion of fossil fuels have been recognized as the primary cause of global warming, presenting a persistent obstacle in the pursuit of the Paris Agreement objectives (Schleussner et al., 2016; Lazarus and van Asselt, 2018). To address this predicament, the utilization of hydrogen as a means of energy storage

from renewable sources has been proposed as a promising remedy for delivering clean fuel and substituting conventional fossil fuels to mitigate carbon emissions (Niaz et al., 2015; Tarkowski, 2019).

Storage of hydrogen in geological formations has become increasingly valued for its capacity to store H<sub>2</sub> on a large scale (Tarkowski, 2019; Zivar et al., 2021; Liu et al., 2022). Hitherto, underground gas storage has been implemented using various locations, such as depleted oil/gas fields, saline aquifers, and salt caverns (Bachu, 2008; Plaat, 2009). Among these

options, the depleted oil field is considered one of the most suitable choices for large-scale H<sub>2</sub> storage because of the well-understood geological factors and the pre-existing facilities (Kanaani et al., 2022).

The safe geological storage of H<sub>2</sub> in depleted hydrocarbon reservoirs requires an understanding of the interfacial tension (IFT) since it is a crucial parameter that plays a significant role in determining the capillary pressure required to seal the migration of H<sub>2</sub> from the storage site through the caprock (Luboń and Tarkowski, 2021; Pan et al., 2021; Hosseini et al., 2022). As the H<sub>2</sub> and oil are not miscible under most geological conditions (Florusse et al., 2003), the H<sub>2</sub>-water-oil three-phase fluid system is involved during H<sub>2</sub> storage in depleted hydrocarbon reservoirs and three types of fluid interfaces, namely, H<sub>2</sub>-water, water-oil, and H<sub>2</sub>-oil interfaces are present. It is important to note that the cushion gas (a non-hydrogen gas) is generally needed to maintain the reservoir pressure during H<sub>2</sub> injection and withdrawal cycles (Heinemann et al., 2022; Kanaani et al., 2022). The presence of cushion gas within geological formations impacts the sealing capillary pressure as a result of unavoidable mixing (Gbadamosi et al., 2023). Therefore, it is imperative to comprehend the impact of impurity gases on the IFT.

The investigations on the effects of impurity gases on the IFT are focused on two-phase mixtures containing H<sub>2</sub> and water (Chow et al., 2018, 2020; Mirchi et al., 2022; Alanazi et al., 2023; Doan et al., 2023; Isfehiani et al., 2023; Muhammed et al., 2023). In general, the interfacial tensions (IFTs) of the impurity gas-H<sub>2</sub>-water two-phase systems under geological conditions decreases with temperature and pressure consistent with results in H<sub>2</sub>-water and impurity gas-water two-phase systems (Chow et al., 2018; Mirchi et al., 2022). It is reported that rising concentrations of N<sub>2</sub> (Muhammed et al., 2023), CH<sub>4</sub> (Mirchi et al., 2022; Alanazi et al., 2023; Doan et al., 2023), or CO<sub>2</sub> (Chow et al., 2018; Isfehiani et al., 2023) as cushion gases leads to decrements of IFTs in the H<sub>2</sub>-H<sub>2</sub>O interface. However, increment of salinity enhances the IFT (Isfehiani et al., 2023; Muhammed et al., 2023).

Recently, Yang et al., 2023c reported the behaviors of IFT in the hydrogen-water-decane three-phase system under reservoir conditions. Their observations show that the IFTs of the H<sub>2</sub>-H<sub>2</sub>O interface in the three-phase mixture are lower compared to the IFTs in the H<sub>2</sub>-H<sub>2</sub>O two-phase mixture. The decrease in IFT is explained by the interfacial accumulation of the C<sub>10</sub>H<sub>22</sub>. Additionally, there is strong adsorption of H<sub>2</sub> in the H<sub>2</sub>O-C<sub>10</sub>H<sub>22</sub> interface in the three-phase system, resulting in less significant increases in IFT as the pressure increases in comparison to those in the H<sub>2</sub>O-C<sub>10</sub>H<sub>22</sub> two-phase mixture. These differences in interfacial properties between the two-phase and the three-phase systems indicate dissimilar effects of impurity gases in the three-phase system in contrast to the above-mentioned results in two-phase systems. However, information regarding the effects of impurity gas on the interfacial behaviors of the hydrogen-water-oil three-phase mixture has not been reported yet.

We utilized the square gradient theory (SGT) coupled to the Perturbed-chain statistical associating fluid theory (PC-SAFT) equation of state (EoS) to study the effects of impurity

gases on the interfacial properties of the H<sub>2</sub>-water-n-decane three-phase mixture under geological conditions. N<sub>2</sub>, CH<sub>4</sub>, and CO<sub>2</sub> were selected as impurity components here as they are typically used as cushion gases (Kanaani et al., 2022; Muhammed et al., 2023). The mole fractions of impurity gas and H<sub>2</sub> were set to be the same to compare the effects of different impurity gas types. The missing parameters for the PC-SAFT SGT modeling of impurity gas-H<sub>2</sub>-H<sub>2</sub>O-n-decane systems were fitted based on solubilities and IFTs of two-component two-phase systems taken from previous experimental studies. In section 2, we presented the details of the methods for PC-SAFT SGT modeling and interfacial property calculations. The results and discussion regarding the effects of impurity gases on three different interfaces under various pressure and temperature condition were presented in Section 3. Finally, the important findings and conclusions were summarized in section 4.

## 2. Method

### 2.1 Equation of state

The estimation of the fluid bulk was conducted using the PC-SAFT equation of state. The equation can be represented through the compressibility factor  $Z$  (Gross and Sadowski, 2001, 2002):

$$Z = 1 + Z^{\text{hc}} + Z^{\text{disp}} + Z^{\text{assoc}} \quad (1)$$

where  $Z^{\text{hc}}$  refers to the hard-chain contribution,  $Z^{\text{disp}}$  refers to the dispersive contribution, and  $Z^{\text{assoc}}$  refers to the part from hydrogen bonds.  $Z$  is dependent on the site number  $m_i$ , the site size  $\sigma_i$ , and the dispersion energy  $\varepsilon_i$ . To capture the interactions resulting from hydrogen bonding between associating molecules, two additional parameters, namely the association energy  $\varepsilon^*$  and association volume  $\kappa$ , were introduced. The H<sub>2</sub>O was modeled with the 4C association scheme and there is no self-association for other components. However, CO<sub>2</sub> can cross-associate with H<sub>2</sub>O (Tsivintzelis et al., 2011). The modeling of H<sub>2</sub>O utilized a 4C association scheme. There was no self-association for other components. But CO<sub>2</sub> can form cross-associations with H<sub>2</sub>O (Tsivintzelis et al., 2011). The parameters for dissimilar sites were determined using the Lorentz-Berthelot combining rules (Gross and Sadowski, 2001):

$$\sigma_{ij} = \frac{1}{2}(\sigma_i + \sigma_j) \quad (2)$$

$$\varepsilon_{ij} = \sqrt{\varepsilon_i \varepsilon_j}(1 - k_{ij}) \quad (3)$$

where  $k_{ij}$  represents the binary interaction parameter. The values for the equation of state parameters were obtained from previous studies (Gross and Sadowski, 2001; Diamantonis and Economou, 2011; Mairhofer and Gross, 2018; Yang et al., 2020, 2023c; Alanazi et al., 2022) or fitted using experimental data (Chapoy et al., 2004). The corresponding parameters are displayed in Tables 1 and 2.

**Table 1.** PC-SAFT EoS parameters for different components.

Components	m	$\sigma$ (Å)	$\epsilon/k$ (K)	$\epsilon^*/k$ (K)	$\kappa$	Reference
H <sub>2</sub>	0.6800	3.5400	31.57	/	/	Alanazi et al., 2022
N <sub>2</sub>	1.2053	3.3130	90.96	/	/	Gross and Sadowski, 2001
CH <sub>4</sub>	1.0000	3.7039	150.03	/	/	Gross and Sadowski, 2001
CO <sub>2</sub>	2.0729	2.7852	169.21	/	/	Gross and Sadowski, 2001
H <sub>2</sub> O	2.1945	2.2290	141.66	1804.17	0.2039	Diamantonis and Economou, 2011
C <sub>10</sub> H <sub>22</sub>	4.6627	3.8384	243.87	/	/	Gross and Sadowski, 2001
CO <sub>2</sub> -H <sub>2</sub> O	/	/	/	902.09	0.5221	Yang et al., 2020

**Table 2.** EoS binary interaction parameters.

Pair	Binary interaction parameter	Reference
H <sub>2</sub> -H <sub>2</sub> O	$-1.0158e-5 \cdot T^2 + 9.1742e-3 \cdot T - 2.1375$	Yang et al., 2023c
N <sub>2</sub> -H <sub>2</sub> O	$-6.6551e-6 \cdot T^2 + 5.9323e-3 \cdot T - 1.1707$	Chapoy et al., 2004*
CH <sub>4</sub> -H <sub>2</sub> O	$-5.2019e-6 \cdot T^2 + 4.5590e-3 \cdot T - 8.1936e-1$	Yang et al., 2020
CO <sub>2</sub> -H <sub>2</sub> O	$3.8257e-4 \cdot T - 2.8007e-2$	Yang et al., 2020
C <sub>10</sub> H <sub>22</sub> -H <sub>2</sub> O	$-3.5305e-6 \cdot T^2 + 2.9134e-3 \cdot T - 3.7739e-1$	Yang et al., 2020
H <sub>2</sub> -C <sub>10</sub> H <sub>22</sub>	$2.5037e-4 \cdot T - 1.9778e-2$	Yang et al., 2023c
N <sub>2</sub> -C <sub>10</sub> H <sub>22</sub>	1.0360e-1	Mairhofer and Gross, 2018
CH <sub>4</sub> -C <sub>10</sub> H <sub>22</sub>	5.6000e-2	Gross and Sadowski, 2001
CO <sub>2</sub> -C <sub>10</sub> H <sub>22</sub>	1.2800e-1	Gross and Sadowski, 2001
N <sub>2</sub> -H <sub>2</sub>	0.0000	/
CH <sub>4</sub> -H <sub>2</sub>	0.0000	/
CO <sub>2</sub> -H <sub>2</sub>	0.0000	/

Notes: The temperature  $T$  is in unit of K, \* denotes the reference of the experimental data for fitting the parameter.

## 2.2 Square gradient theory

The three-phase fluid mixture contains three interfaces as shown in Fig. 1(a). Note that the mole fraction of impurity gas is set to be the same as H<sub>2</sub> for all the calculations in this study. The PC-SAFT EoS was combined with the SGT to calculate interfacial properties of the gas-water, water-oil, and gas-oil interfaces, separately. In the formulation of the SGT, the Helmholtz free energy for a planar interface with an area of  $A$  is expressed as (Davis and Scriven, 1982; Davis, 1996):

$$F = A \int_{-\infty}^{+\infty} \left[ f_0(n) + \frac{1}{2} \sum_i \sum_j c_{ij} \frac{dn_i(z)}{dz} \frac{dn_j(z)}{dz} \right] dz \quad (4)$$

where  $f_0$  represents the Helmholtz free energy density of the bulk fluid,  $n$  refers to the bulk density, and  $dn_i(z)/dz$  denotes the gradient of the local density of the  $i^{\text{th}}$  component. The cross influence parameter, denoted as  $c_{ij}$ , is defined as (Cornelisse et al., 1993; Miqueu et al., 2011):

$$c_{ij} = (1 - \beta_{ij}) \sqrt{c_{ii} c_{jj}} \quad (5)$$

where  $c_{ii}/c_{jj}$  denote the influence parameters of pure species, and  $\beta_{ij}$  refers to the binary interaction coefficient. The above parameters were taken from the literature (Mairhofer and Gross, 2018; Yang et al., 2020, 2023b, 2023c) or fitted using experimental data (Wiegand and Franck, 1994; Sachs and Meyn, 1995; Linstrom and Mallard, 2001; Kashefi et al., 2016; Pereira et al., 2016b). The parameters are presented in Tables 3 and 4. Here, non-zero  $\beta_{ij}$  values for gas-oil and gas-gas pairs are used to maintain the stability of the calculation.

To determine the equilibrium density profiles across the interface, the Helmholtz free energy was minimized by solving the corresponding Euler-Lagrange equation (Davis and Scriven, 1982; Davis, 1996):

$$\sum_j c_{ij} \frac{d^2 n_j(z)}{dz^2} = \mu_i(n_1(z), \dots, n_{N_c}(z)) - \mu_i^0 \quad \text{for } i, j = 1, \dots, N_c \quad (6)$$

where  $\mu_i^0$  refers to the chemical potential of the  $i^{\text{th}}$  component in the bulk phase. It is defined as the partial derivative of  $f_0$  with respect to  $n_i$ , while keeping temperature, volume, and the densities of other components constant.  $\mu_i$  refers to the chem-

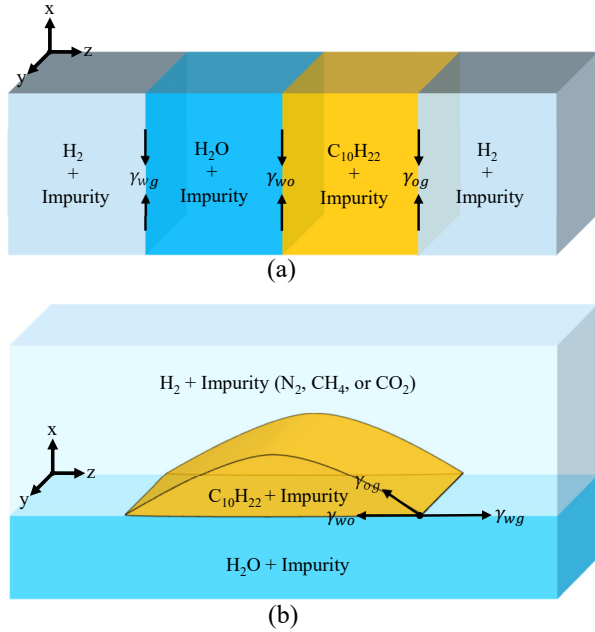


**Fig. 1.** (a) Impurity gas-H<sub>2</sub>-H<sub>2</sub>O-C<sub>10</sub>H<sub>22</sub> three-phase system and (b) spreading of a cylindrical oil droplet.

**Table 3.** SGT influence parameters for different components.

Component	Influence parameter (10 <sup>-20</sup> J·m <sup>5</sup> ·mol <sup>-2</sup> )	Reference
H <sub>2</sub>	0.0350	Yang et al., 2023b
N <sub>2</sub>	1.0615	Linstrom and Mallard, 2001*
CH <sub>4</sub>	1.6736	Yang et al., 2020
CO <sub>2</sub>	2.4280	Yang et al., 2020
H <sub>2</sub> O	1.4412	Mairhofer and Gross, 2018
C <sub>10</sub> H <sub>22</sub>	90.8954	Yang et al., 2020

Notes: \* denotes the reference of the experimental data for fitting the parameter.

ical potential of the  $i^{\text{th}}$  component, and  $N_c$  represents the total number of components. The finite difference method was employed to discretize the nonlinear equations, which were then solved using the Newton-Raphson iteration method with an in-house code (Yang et al., 2023a). A total of 200 evenly spaced grid points were utilized for the computation. Initially, the interfacial thickness ( $l$ ) is assumed to be 15 Å. Subsequently, it is progressively increased until the convergence of IFT (Davis and Scriven, 1982; Davis, 1996).

The boundary conditions for SGT are calculated using the 3-phase flash method with PC-SAFT EoS (Rachford and Rice, 1952; Pan et al., 2019):

$$\begin{aligned} n_i &= n_i^I \text{ at } z = 0, \\ n_i &= n_i^{II} \text{ at } z = l \end{aligned} \quad (7)$$

where  $n_i^I$  and  $n_i^{II}$  denote the densities of the bulk phase  $I$  and  $II$ , separately.

### 2.3 Interfacial properties

Once the equilibrium spatial distributions were obtained, the interfacial tension ( $\gamma$ ) can be estimated using the following formula (Davis and Scriven, 1982; Davis, 1996):

$$\gamma = \int_{-\infty}^{+\infty} \sum_i \sum_j c_{ij} \frac{dn_i(z)}{dz} \frac{dn_j(z)}{dz} dz \quad (8)$$

In order to verify the modeling parameters, the IFTs from PC-SAFT SGT predictions are compared to experimental data of the gas-H<sub>2</sub>O (Wiegand and Franck, 1994; Sachs and Meyn, 1995; Chow et al., 2016, 2018, 2020; Kashefi et al., 2016; Pereira et al., 2016b), the H<sub>2</sub>O-decane (Georgiadis et al., 2011), and the gas-decane (Stegemeier et al., 1962; Amin and Smith, 1998; Linstrom and Mallard, 2001; Georgiadis et al., 2010, 2016c; Pan and Trusler, 2023b) two-phase systems. This comparison is illustrated in Figs. A1-A3. The predictions derived from SGT align well with the experiment measurements.

Enrichment can be used to gauge the non-monotonic characteristics of component density profiles (Becker et al., 2016; Stephan et al., 2023):

$$E_i = \frac{\max(n_i(z))}{\max(n_i^I, n_i^{II})} \quad (9)$$

The behaviors of IFT are connected to the surface excesses through the Gibbs adsorption equation (Miqueu et al., 2011; Radke, 2015; Stephan and Hasse, 2020):

$$-d\gamma = \sum_i \Gamma_{i,j} d\mu_i \quad (10)$$

where  $\Gamma_{i,j}$  refers to the surface excess of species  $i$  with the reference species  $j$ . The surface excesses are calculated by (Telo da Gama and Evans, 1983; Wadewitz and Winkelmann, 1996):

$$\Gamma_{i,j} = -(n_i^{II} - n_i^I) \int_{-\infty}^{+\infty} \left[ \frac{n_j(z) - n_j^{II}}{n_j^{II} - n_j^I} - \frac{n_i(z) - n_i^{II}}{n_i^{II} - n_i^I} \right] dz \quad (11)$$

where  $I$  represents the phase enriched with component  $i$  and  $II$  represents the phase enriched with component  $j$ .

The spreading coefficient  $S$  can be utilized as a measure to ascertain if the oil possesses the capability to create a thin film that spreads between different phases (Harkins and Feldman, 1922; Shaw, 1980):

$$S = \gamma_{wg} - \gamma_{wo} - \gamma_{og} \quad (12)$$

where  $\gamma_{wg}$ ,  $\gamma_{wo}$ , and  $\gamma_{og}$  denote the IFT of the water-gas interface, the oil-water interface, the gas-oil interface, separately. If  $S$  is positive, it suggests that the oil film has the capability to spread, creating a new oil phase that separates the water-rich and gas-rich phases due to the reduction in interfacial free energy. However, if  $S$  is negative, it signifies the formation of an oil lens instead (Bertrand et al., 2001; Bonn et al., 2009) as shown in Fig. 1(b).

**Table 4.** SGT binary interaction coefficients for pairs.

Pair	Binary interaction coefficient	Reference
H <sub>2</sub> -H <sub>2</sub> O	0.99	Yang et al., 2023c
N <sub>2</sub> -H <sub>2</sub> O	$1.9523e-5 \cdot T^2 - 1.7855e-2 \cdot T + 4.4372$	Wiegand and Franck, 1994*
CH <sub>4</sub> -H <sub>2</sub> O	$2.4957e-5 \cdot T^2 - 2.0171e-2 \cdot T + 4.4999$	Sachs and Meyn, 1995*; Kashefi et al., 2016*
CO <sub>2</sub> -H <sub>2</sub> O	$-1.3849e-5 \cdot T^2 + 8.4506e-3 \cdot T - 7.5763e-1$	Pereira et al., 2016b*
C <sub>10</sub> H <sub>22</sub> -H <sub>2</sub> O	$7.5941e-6 \cdot T^2 - 6.4833e-3 \cdot T + 1.7825$	Yang et al., 2023c
Gas-C <sub>10</sub> H <sub>22</sub>	0.20	/
Gas-gas	0.25	/

Notes: \* denotes the reference of the experimental data for fitting the parameter.

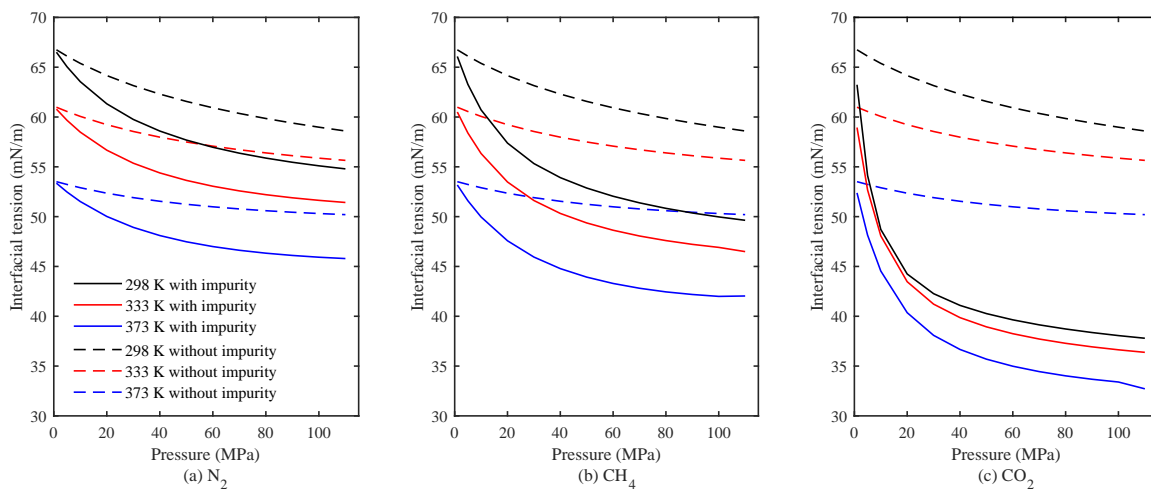


**Fig. 2.** Interfacial tensions of the H<sub>2</sub>-H<sub>2</sub>O interface. Dashed lines are from Yang et al. (2023c).

### 3. Results and discussion

#### 3.1 Hydrogen-water interface

We first investigate the H<sub>2</sub>-H<sub>2</sub>O interface in the gas-H<sub>2</sub>-H<sub>2</sub>O-C<sub>10</sub>H<sub>22</sub> three-phase systems. The IFT results of the interface are displayed in Fig. 2 for systems containing (a) N<sub>2</sub>, (b) CH<sub>4</sub>, and (c) CO<sub>2</sub>. It is observed that the IFT values reduce with rising temperature and pressure in line with the corresponding trends from the three-phase system without impurity gas plotted together as dashed lines (Yang et al., 2023c). It can be known that the presence of impurity gas weakens the IFT of the interface. Similar reductions of IFT have been reported in the H<sub>2</sub>-H<sub>2</sub>O two-phase systems in contact with N<sub>2</sub>, CH<sub>4</sub>, and/or CO<sub>2</sub> (Chow et al., 2018; Mirchi et al., 2022; Muhammed et al., 2023; Doan et al., 2023; Isfehiani et al., 2023). The results in systems with CH<sub>4</sub> and CO<sub>2</sub> are also respectively consistent with observations in the CH<sub>4</sub>-H<sub>2</sub>O-C<sub>10</sub>H<sub>22</sub> (Bahramian et al., 2007; Pereira et al., 2014, 2016a; Yang et al., 2022) and the CO<sub>2</sub>-H<sub>2</sub>O-C<sub>10</sub>H<sub>22</sub> (Yang et al., 2023a) three-phase systems under much narrower pressure ranges. Moreover, the decrement of IFT is pronounced at elevated pressures. The amount of reduction depends on the

type of impurity gas following this order: CO<sub>2</sub> > CH<sub>4</sub> > N<sub>2</sub>.

The species density distributions in the hydrogen-water interface in the gas-H<sub>2</sub>-H<sub>2</sub>O-C<sub>10</sub>H<sub>22</sub> three-phase systems at various conditions are presented in Fig. 3. The density profiles of H<sub>2</sub>, H<sub>2</sub>O, and C<sub>10</sub>H<sub>22</sub> in the presence of impurity gas show resemblance to the density profiles observed in the corresponding three-phase system without the impurity gas (as depicted in Fig. A4) (Yang et al., 2023c). An anticipated trend is observed where the H<sub>2</sub>O density gradually decreases from the water-rich phase to the gas-rich phase. In the interfacial region, there are peaks in the densities of H<sub>2</sub> and C<sub>10</sub>H<sub>22</sub>. Importantly, strong adsorptions of N<sub>2</sub>, CH<sub>4</sub>, and CO<sub>2</sub> are observed in the interfacial region in contrast to those of H<sub>2</sub>. The adsorption of gases in the H<sub>2</sub>O-gas interface has been reported in previous studies on other multiphase fluid systems (Miqueu et al., 2011; Yang et al., 2023a; Doan et al., 2023). Further, this adsorption tends to decrease with elevated temperatures.

The solubility of species in the bulk region of the aqueous and the H<sub>2</sub>-rich phases are given in Figs. A5 and A6. It is seen that the presence of impurity gases decreases the solubilities of H<sub>2</sub> and decane in the aqueous phase, especially under high pressure and temperature conditions. On the other hand, the

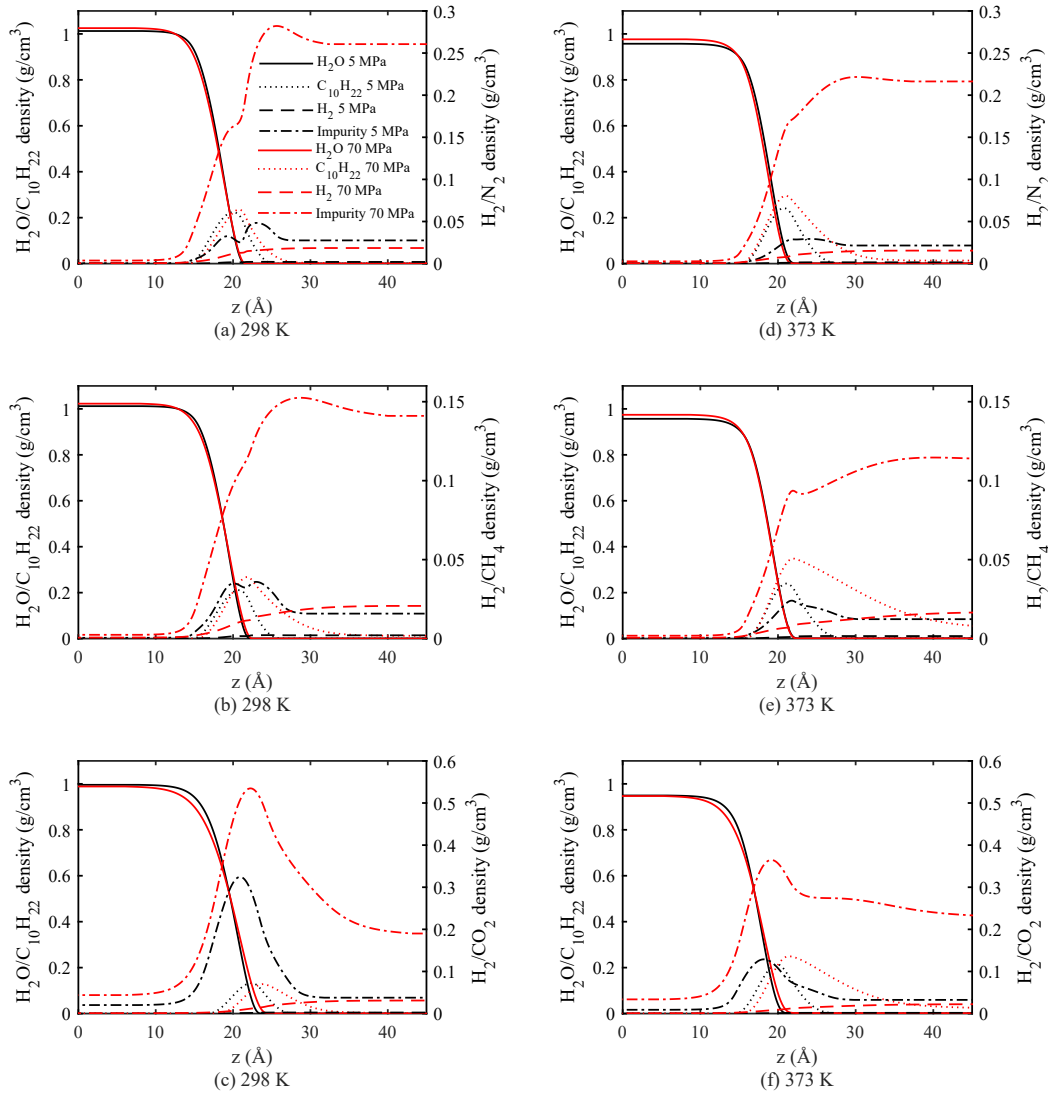


**Fig. 3.** Component density distributions of the H<sub>2</sub>-H<sub>2</sub>O interface.

presence of impurity gases enhances the solubilities of decane in the H<sub>2</sub>-rich phase at elevated pressures, while the H<sub>2</sub>O solubilities are hardly influenced by the impurity gases.

The corresponding component enrichments are displayed in Fig. 4. The enrichments of different species are weakened with rising pressure and temperature and generally converge to one at high pressure and temperature conditions. The enrichments of H<sub>2</sub> and decane show similar trends as those in the three-phase system without impurity gas (see dashed lines) (Yang et al., 2023c). The presence of impurity gases weakens the enrichments of other species. The enrichments of impurity gases follow this sequence: CO<sub>2</sub> > CH<sub>4</sub> > N<sub>2</sub>. This sequence is likely associated with the interaction energies between gases and water. The strongest CO<sub>2</sub>-H<sub>2</sub>O interaction arises from the quadrupole-dipole interactions. Remarkably, it has been shown from a molecular simulation study that carbon dioxide can bond to water forming stable “T-shaped” structure in the interfacial region, which enhances the enrichment of CO<sub>2</sub> (Makimura et al., 2013). The weaker CH<sub>4</sub>/N<sub>2</sub>-H<sub>2</sub>O interactions

are due to the relatively small van der Waals interactions.

The surface excesses are presented in Fig. 5. Consistent with results without impurity gases (dashed lines) (Yang et al., 2023c), the H<sub>2</sub> surface excesses are mostly negative and generally decrease with pressure and temperature. The presence of N<sub>2</sub> enhances H<sub>2</sub> surface excesses, particularly at high temperatures. However, CH<sub>4</sub> and CO<sub>2</sub> reduce the H<sub>2</sub> surface excesses. Meanwhile, the decane surface excess is generally positive and increases with rising pressure and temperature similar to the case without impurity gases (Yang et al., 2023c). The increased decane surface excess is likely associated with the greater decane solubility in the H<sub>2</sub>-rich phase at higher temperatures and pressures (see Fig. A6). Impurity gases generally rise the surface excess of decane. However, in the CO<sub>2</sub> case, reductions of decane surface excesses are seen at relatively low pressures and temperatures. Moreover, surface excesses of N<sub>2</sub> and CH<sub>4</sub> increase with pressure at low pressures and then decrease with pressure at high pressures. However, CO<sub>2</sub> surface excesses increase with

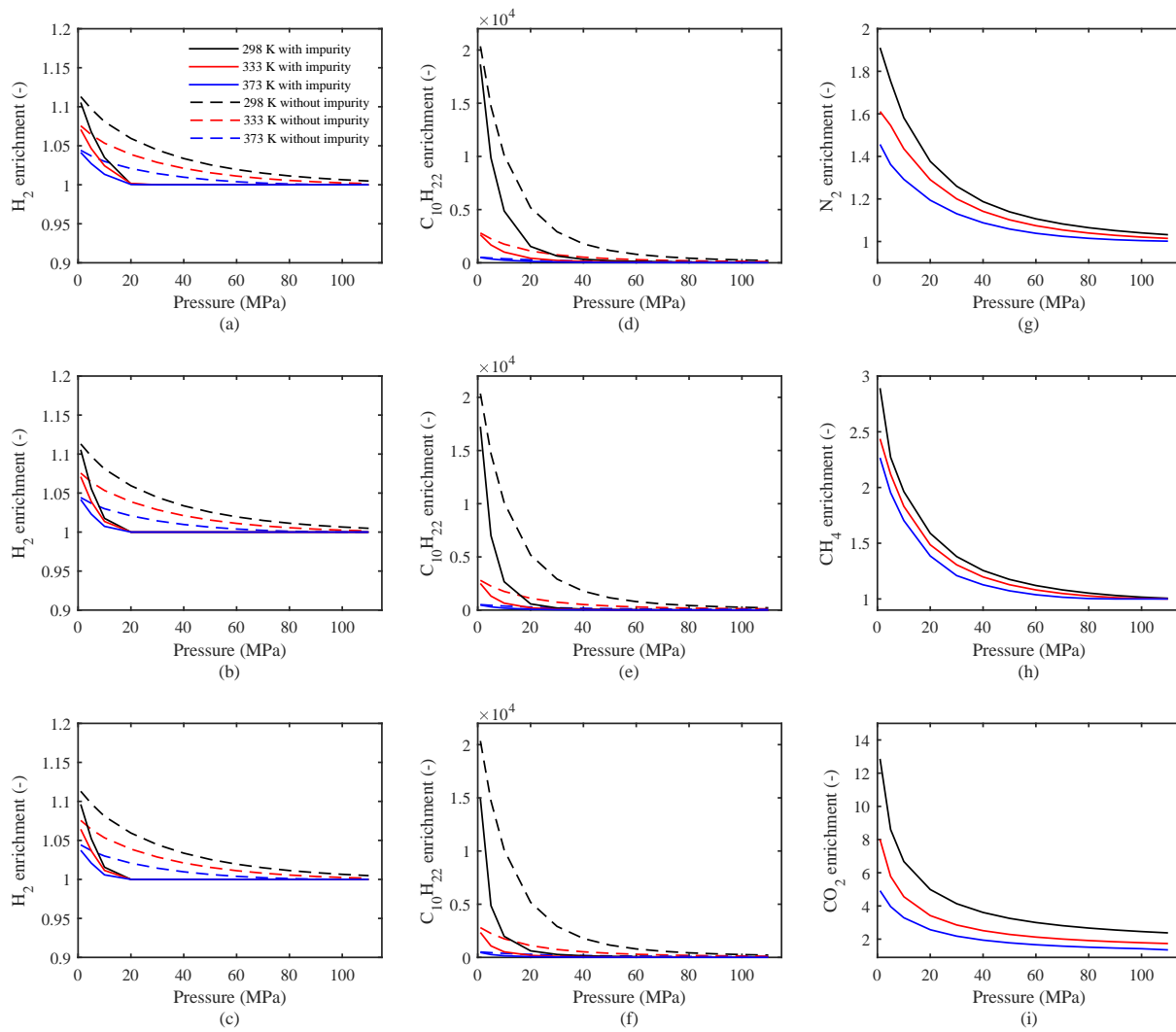


**Fig. 4.** Component enrichments of the H<sub>2</sub>-H<sub>2</sub>O interface. Top, middle, and bottom panels show enrichments in systems containing N<sub>2</sub>, CH<sub>4</sub>, and CO<sub>2</sub>, respectively. Dashed lines are taken from Yang et al. (2023c).

pressure and then reach plateaus at relatively high pressures. Nevertheless, the surface excesses of impurity gas decline with rising temperature.

The behaviors of component surface excesses are usually used to explain the trends of IFT values (Miqueu et al., 2011; Li and Jin, 2019). According to the Gibbs adsorption equation (i.e., Eq. (10)), the reductions of IFT with pressure are associated with positive surface excesses of components, while the increments of IFT are linked to negative surface excesses. Hence, the reductions of IFTs in contrast to the system without impurity gases can be mainly explained by the combined effects of positive surface excesses of impurity gases (only at low-pressure regions for N<sub>2</sub> and CH<sub>4</sub> systems) and enhanced surface excesses of decane (only at high temperatures for the CO<sub>2</sub> system), while the negative surface excesses contribute negatively to the reductions of IFT.

### 3.2 Water-decane interface

We then study the H<sub>2</sub>O-C<sub>10</sub>H<sub>22</sub> interface in the gas-H<sub>2</sub>-H<sub>2</sub>O-C<sub>10</sub>H<sub>22</sub> three-phase systems. The IFT results of the

interface are displayed in Fig. 6. The corresponding IFTs weaken at elevated temperatures in all cases. In the system with N<sub>2</sub>, the IFTs change moderately with pressure. Nevertheless, IFTs decrease with pressure at 298 K, while opposite pressure effects are seen at higher temperatures. Meanwhile, in systems with CH<sub>4</sub> and CO<sub>2</sub>, the IFT values reduce greatly with rising pressure. The results without impurity gases are plotted together as dashed lines (Yang et al., 2023c). By comparing solid and dashed lines, it is known that the presence of impurity gases also weakens the IFTs in the H<sub>2</sub>O-C<sub>10</sub>H<sub>22</sub> interfaces, and the amount of reduction follows this order: CO<sub>2</sub> > CH<sub>4</sub> > N<sub>2</sub>. The IFT values are consistent with the IFT data for the H<sub>2</sub>O-C<sub>10</sub>H<sub>22</sub> interface containing CH<sub>4</sub> or CO<sub>2</sub> in the absence of H<sub>2</sub> in two-phase systems under miscible conditions (Jennings Jr and Newman, 1971; Georgiadis et al., 2011; Yang et al., 2020), and three-phase systems under immiscible conditions (Bahramian et al., 2007; Pereira et al., 2014, 2016a; Yang et al., 2022, 2023a; Pan and Trusler, 2023a).

The species density distributions in the water-oil interface in the gas-H<sub>2</sub>-H<sub>2</sub>O-C<sub>10</sub>H<sub>22</sub> three-phase systems at various

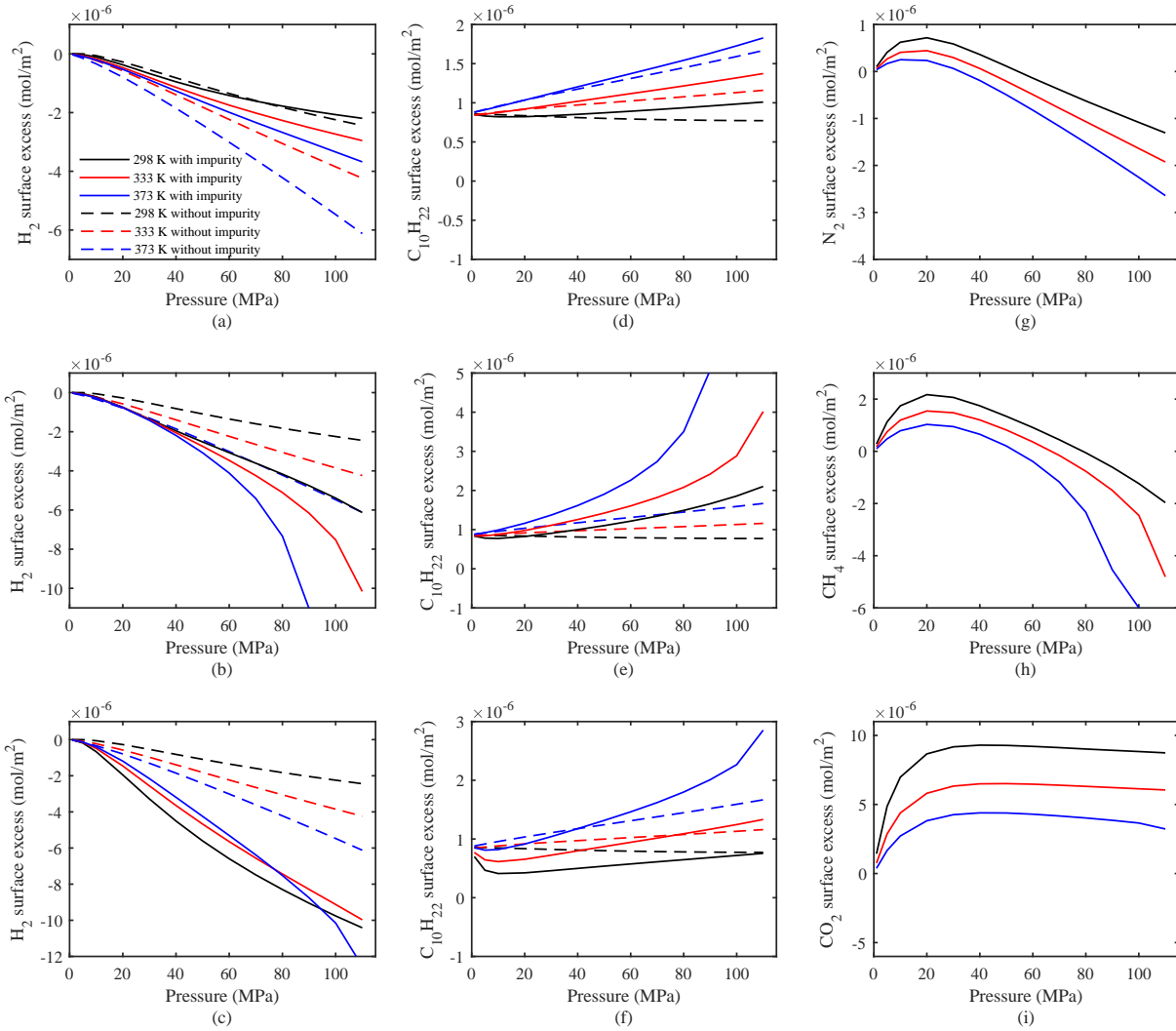


**Fig. 5.** Component surface excesses of the H<sub>2</sub>-H<sub>2</sub>O interface. Top, middle, and bottom panels show surface excesses in systems containing N<sub>2</sub>, CH<sub>4</sub>, and CO<sub>2</sub>, respectively. Dashed lines are taken from Yang et al. (2023c).

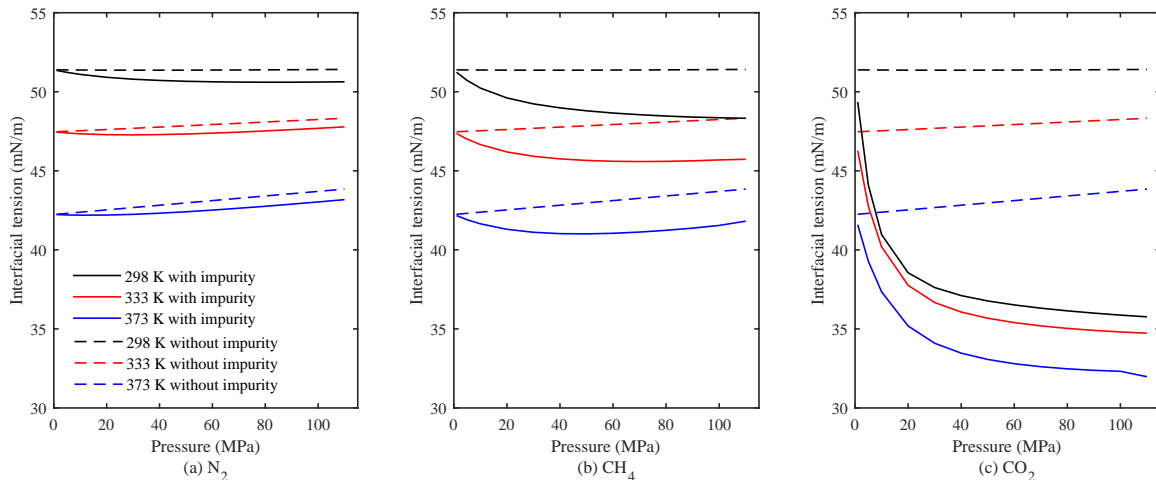


**Fig. 6.** Interfacial tensions of the H<sub>2</sub>O-C<sub>10</sub>H<sub>22</sub> interface. Dashed lines are from Yang et al. (2023c).



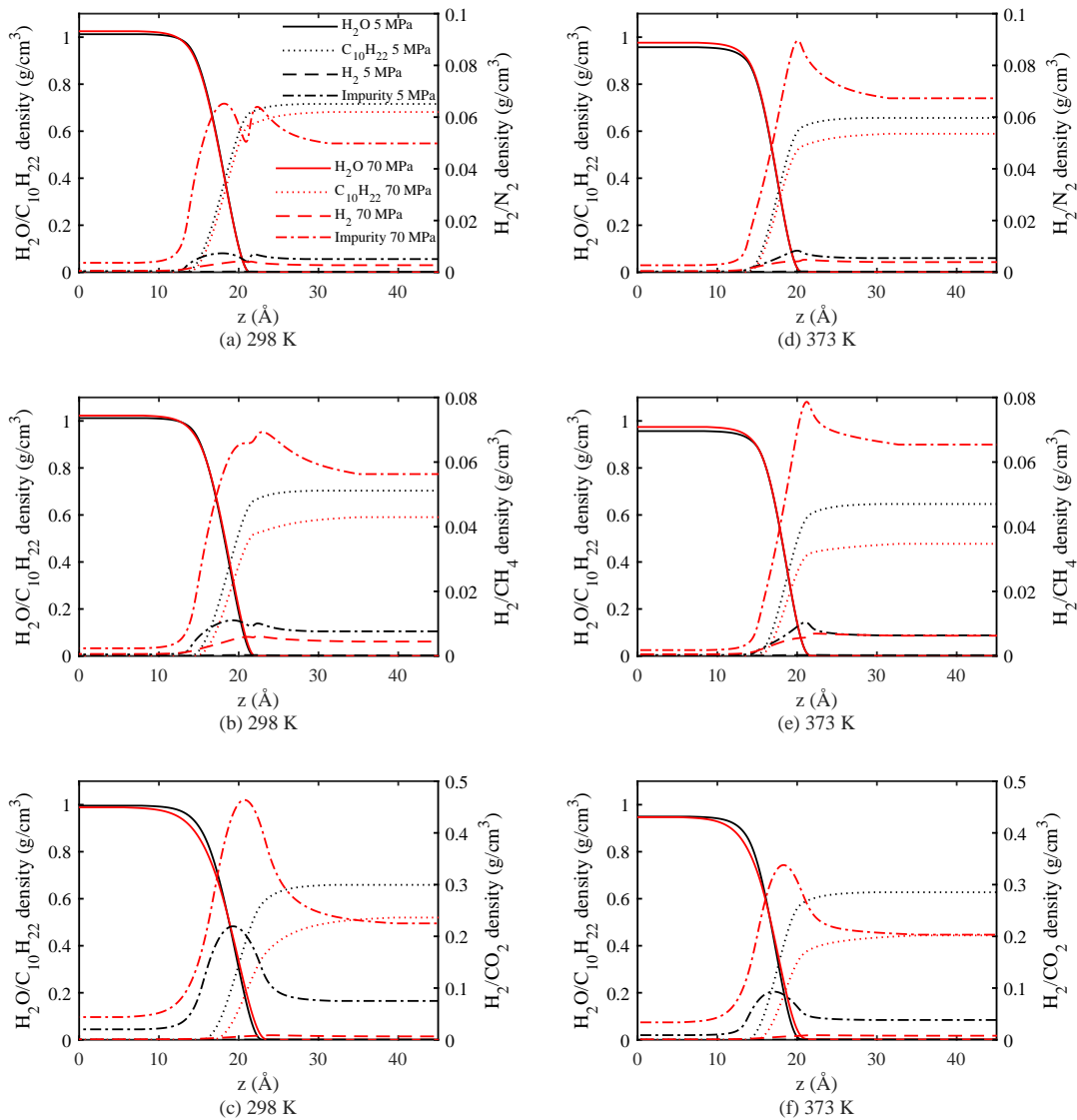


**Fig. 7.** Component density distributions of the  $\text{H}_2\text{O}-\text{C}_{10}\text{H}_{22}$  interface.

conditions are presented in Fig. 7. The density distributions of  $\text{H}_2$ ,  $\text{H}_2\text{O}$ , and  $\text{C}_{10}\text{H}_{22}$  in the presence of impurity gas exhibit similarity to those observed in the corresponding three-phase system without the impurity gas (as depicted in Fig. A7) (Yang et al., 2023c). As expected, the density profiles of  $\text{H}_2\text{O}$  and decane monotonically vary from one phase to the other phase. In the interfacial region, there are peaks in the densities of gases and the adsorptions of  $\text{N}_2$ ,  $\text{CH}_4$ , and  $\text{CO}_2$  in the interfacial region are much larger than those of  $\text{H}_2$ . The adsorption of gases in the  $\text{H}_2\text{O}$ -oil interface has been reported in simulation studies on other multiphase fluid systems (Yang et al., 2020, 2022, 2023a).

The solubility of species in the decane-rich phases is given in Fig. A8. In general, the solubilities of impurity gases generally increase pressure. However, in the  $\text{CO}_2$  case under high pressures ( $>$  around 30 MPa), the  $\text{CO}_2$  solubility declines with pressure. Meanwhile, high temperature increases the  $\text{N}_2$  solubility and decreases the  $\text{CO}_2$  solubility (Hemmati-Sarapardeh et al., 2014; Karkevandi-Talkhooncheg et al., 2018;

Peng et al., 2018). And the effect of temperature on  $\text{CH}_4$  solubility is moderate. On the other hand, it is seen that the presence of impurity gases decreases the solubilities of  $\text{H}_2$  in the decane-rich phase, especially under high-pressure conditions. Interestingly, impurity gases have the effect of increasing water solubility in systems containing  $\text{CO}_2$ , while reducing water solubility in systems containing  $\text{N}_2$  and  $\text{CH}_4$ .

The component enrichment results are shown in Fig. 8. The enrichments of impurity gases decline with pressure. In general, high temperature enhances the enrichment of  $\text{N}_2$  and declines the enrichment of  $\text{CO}_2$ . In the  $\text{CH}_4$  case, there is a transition point located at around 65 MPa for the pressure effect on the enrichment. At pressure lower than 65 MPa,  $\text{CH}_4$  enrichments increase with temperature while an opposite temperature effect is observed at higher pressures. The  $\text{H}_2$  enrichments decrease with pressure and temperature. The presence of impurity gas reduces the enrichments of  $\text{H}_2$  in contrast to cases without impurity gas (see dashed lines (Yang et al., 2023c)). The effects of  $\text{CH}_4$  and  $\text{CO}_2$  on  $\text{H}_2$  enrichment

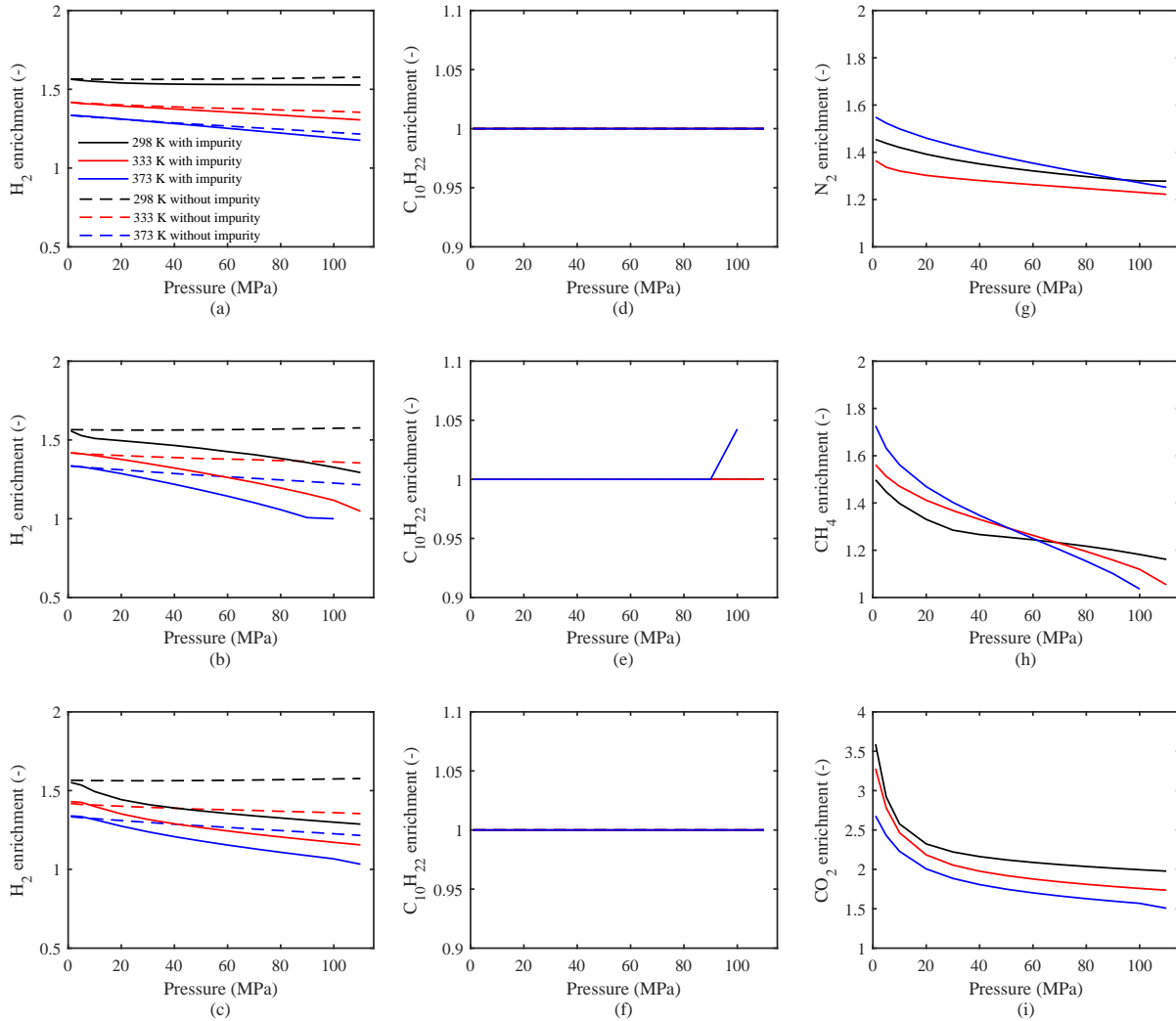


**Fig. 8.** Component enrichments of the  $\text{H}_2\text{O}-\text{C}_{10}\text{H}_{22}$  interface. Top, middle, and bottom panels show enrichments in systems containing  $\text{N}_2$ ,  $\text{CH}_4$ , and  $\text{CO}_2$ , respectively. Dashed lines are taken from Yang et al. (2023c).

are greater than that of  $\text{N}_2$ . Moreover, the decane enrichments are close to one in all cases.

The corresponding surface excesses are given in Fig. 9. The surface excesses of impurity gases are all positive, and their values follow this sequence:  $\text{CO}_2 > \text{CH}_4 > \text{N}_2$ . Further, the surface excess values decrease with temperature. High pressure generally enhances the surface excesses of  $\text{N}_2$  and  $\text{CO}_2$ . In the  $\text{CH}_4$  case, maximum values of enrichments are observed at relatively high temperatures. Consistent with results without impurity gases (dashed lines) for this interface (Yang et al., 2023c), the  $\text{H}_2$  surface excesses are mostly positive and generally decrease with temperature. The positive surface excess of  $\text{H}_2$  can be explained by the strong energetic interaction between water and hydrogen leading to the adsorption of  $\text{H}_2$  in the interfacial region. The presence of impurity gases reduces the  $\text{H}_2$  surface excess, and the reductions are stronger at higher pressures. Meanwhile, the surface excesses of decane are all negative. Impurity gases generally move the decane surface excess curves downwards. However, at high temperature and pressure conditions, the decane surface excesses become larger

when  $\text{CH}_4$  is added to the system. Based on the above findings, the reduction of IFTs of the water-decane interface in contact with impurity gases can be mainly explained by the strong surface excesses of impurity gases in the interfacial regions.

### 3.3 Hydrogen-Decane Interface

The IFT results for the hydrogen-decane interface are demonstrated in Fig. 10, which are also compared to those in system without impurity gases (Yang et al., 2023c). The values of IFT drop significantly after adding the impurity gases into the system. The reduction of IFT enhances with pressure and changes moderately with temperature. The decrements of IFT caused by the impurity gases follow this order:  $\text{CO}_2 \approx \text{CH}_4 > \text{N}_2$ . Remarkably, the minimum miscibility pressure (MMP) can be obtained as the pressure at which the IFT reaches zero (Ayirala et al., 2006). Our results show that the MMP for the decane-rich and hydrogen-rich phases are beyond 100 MPa in the studied systems. As the IFT reduces with impurity gases, the MMP value also reduces, which is consistent with the reported small MMP values in the  $\text{CH}_4/\text{CO}_2$ -oil two-phase

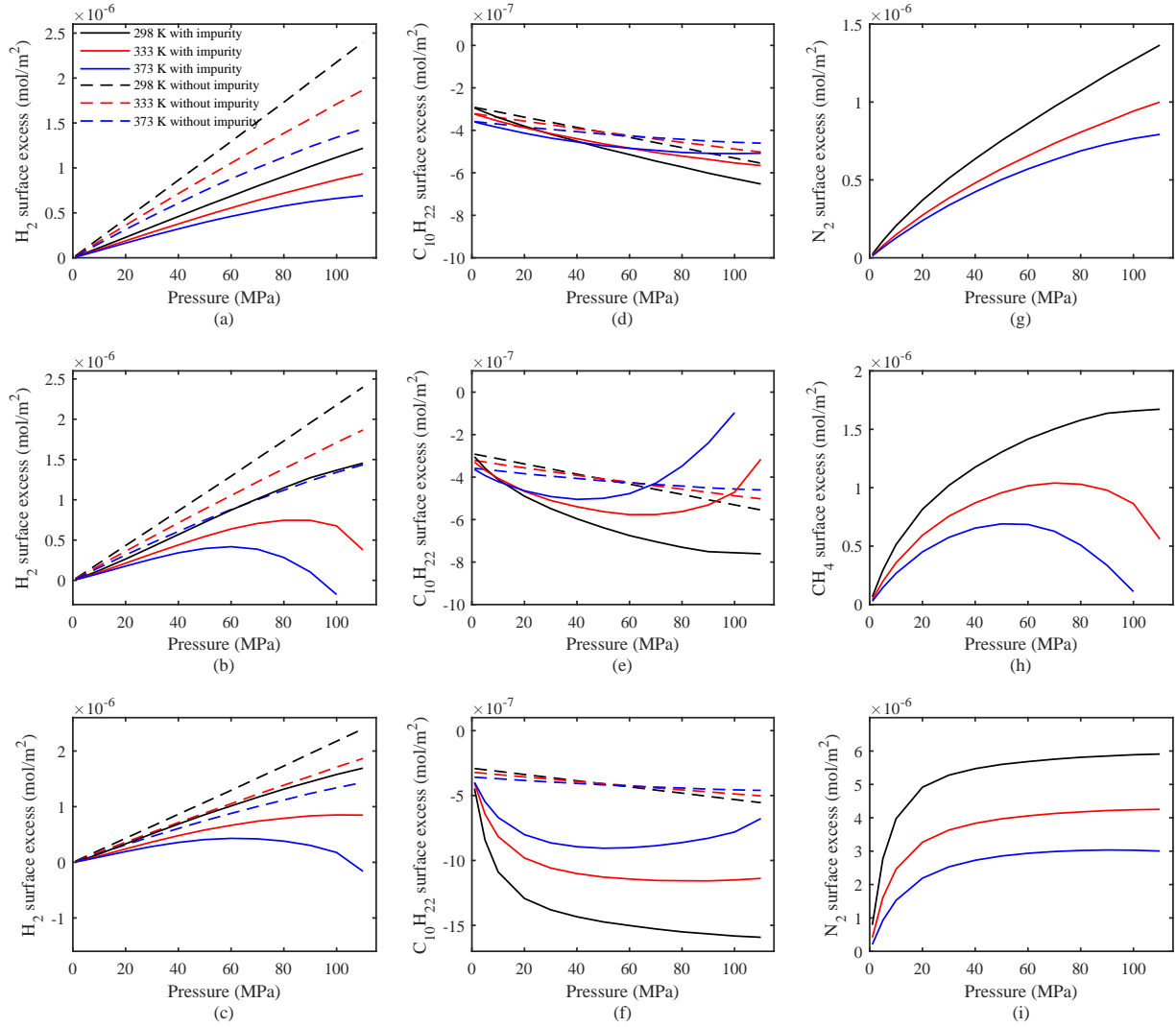


**Fig. 9.** Component surface excesses of the  $\text{H}_2\text{O}-\text{C}_{10}\text{H}_{22}$  interface. Top, middle, and bottom panels show surface excesses in systems containing  $\text{N}_2$ ,  $\text{CH}_4$ , and  $\text{CO}_2$ , respectively. Dashed lines are taken from Yang et al. (2023c).

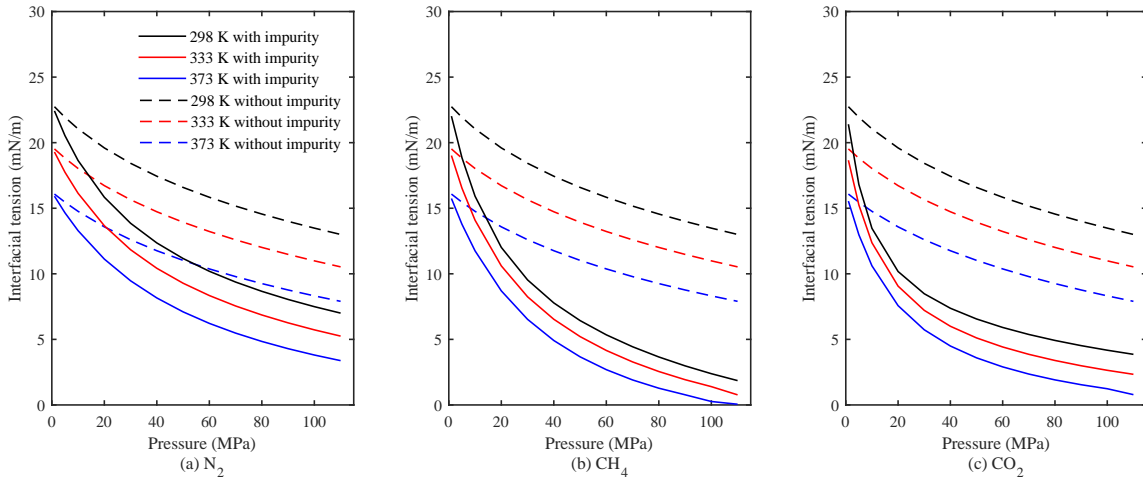


**Fig. 10.** Interfacial tensions of the  $\text{H}_2-\text{C}_{10}\text{H}_{22}$  interface. Dashed lines are from Yang et al. (2023c).

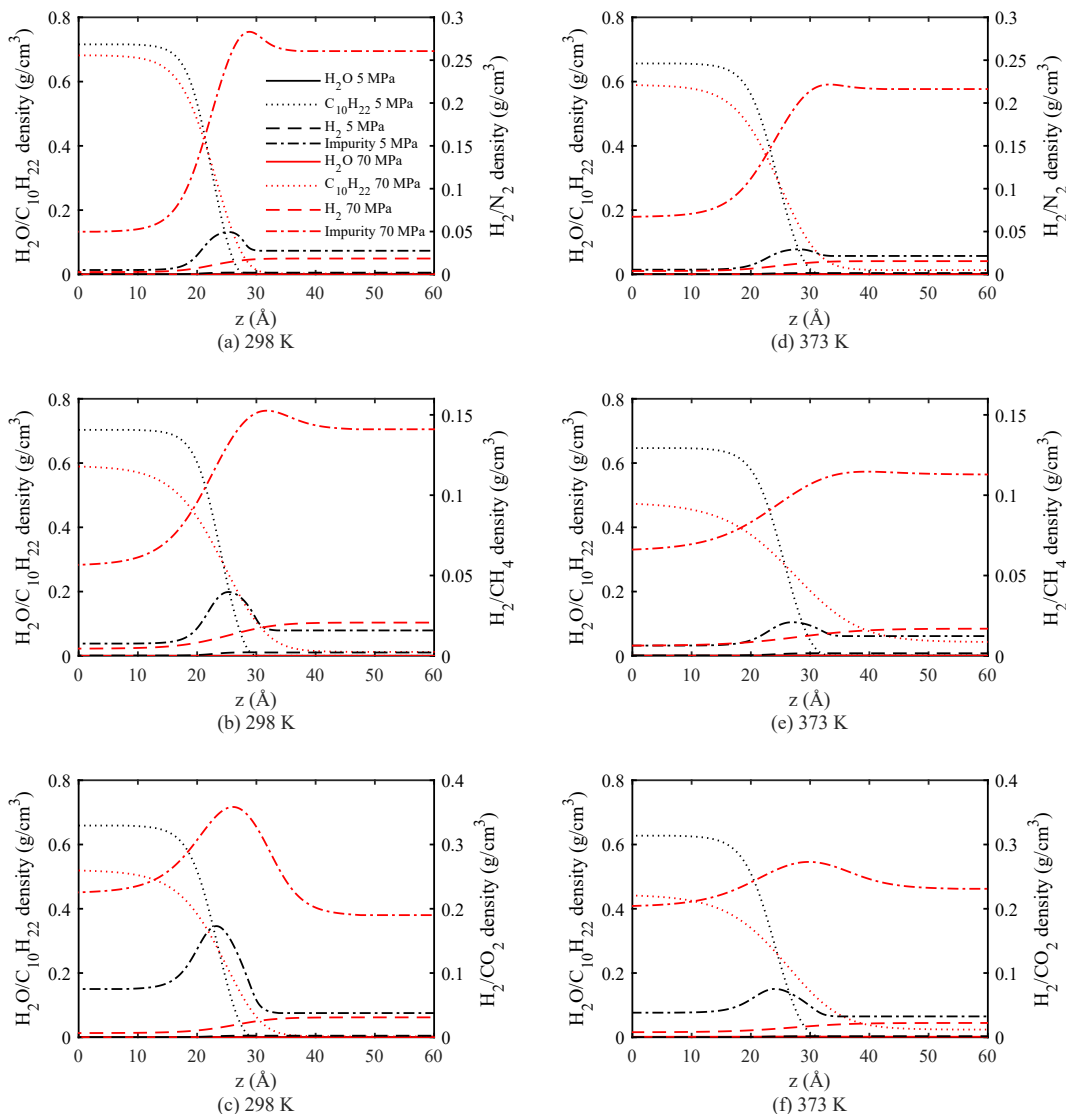


Fig. 11. Component density distributions of the  $H_2$ - $C_{10}H_{22}$  interface.

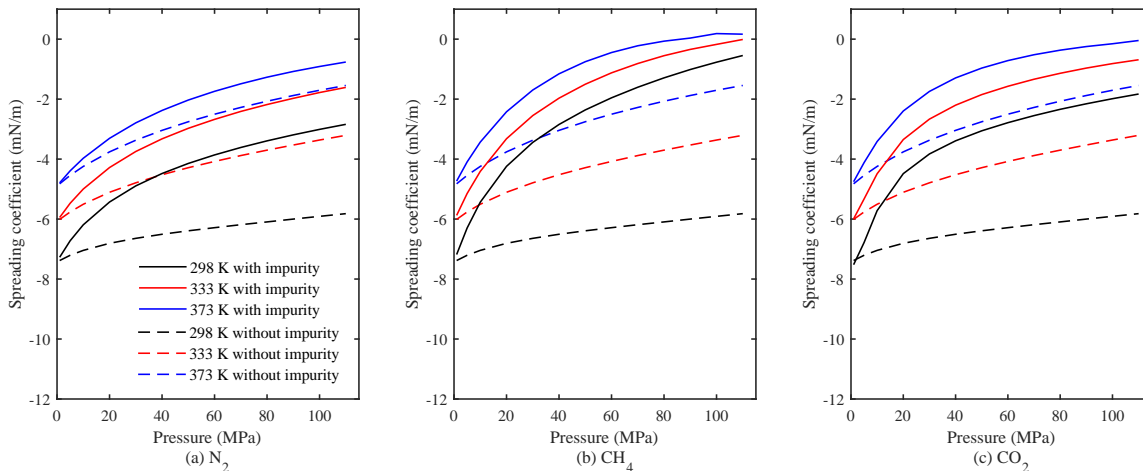


Fig. 12. Spreading coefficients in the gas- $H_2$ - $H_2O$ - $C_{10}H_{22}$  3-phase systems. Dashed lines are taken from Yang et al. (2023c).

systems (Yellig and Metcalfe, 1980; Rao and Lee, 2003).

The species density distributions in the hydrogen-oil interface in the gas-H<sub>2</sub>-H<sub>2</sub>O-C<sub>10</sub>H<sub>22</sub> three-phase systems at various conditions are presented in Fig. 11. The density distributions of H<sub>2</sub>, H<sub>2</sub>O, and C<sub>10</sub>H<sub>22</sub> in the presence of impurity gas are similar to those in the corresponding three-phase system without the impurity gas (see Fig. A9) (Yang et al., 2023c). The densities of water are small in contrast to other components due to its low solubilities in the decane-rich and hydrogen-rich phases (see Figs. A6 and A8). The density profiles of decane monotonically decrease from the decane-rich phase to the hydrogen-rich phase, while density peaks in the interfacial densities of gases are observed in line with previous studies on gas-oil interfaces (Pereira et al., 2016c; Choudhary et al., 2019; Yang et al., 2022, 2023a). Furthermore, the adsorptions of impurity gases are greater than that of H<sub>2</sub>.

The component enrichment data for the hydrogen-decane interface are shown in Fig. A10. For all species in this interface, the enrichments weaken with rising temperature and pressure. The enrichments of impurity gases are greater than those of H<sub>2</sub>, and have similar magnitude to those of water. It is observed that the presence of impurity gases generally reduces the enrichments of H<sub>2</sub> and H<sub>2</sub>O in contrast to cases without impurity gases (see dashed lines) (Yang et al., 2023c). However, the H<sub>2</sub>O enrichments are enhanced by CO<sub>2</sub> (see Fig. A10(f)).

The results for surface excesses are presented in Fig. A11. The surface excesses of impurity gases are all positive and reduce with rising temperature. As pressure rises, the surface excesses values incline first and then decline, and peak at around 40 MPa. The magnitudes also follow this order: CO<sub>2</sub> > CH<sub>4</sub> > N<sub>2</sub>. Meanwhile, adding the impurity gases into the systems leads to significant reductions in H<sub>2</sub> surface excesses, and these reductions change the sign of H<sub>2</sub> from positive to negative by comparing the solid lines with results in the system without impurity gases (dashed lines) (Yang et al., 2023c). The H<sub>2</sub>O surface excesses are reduced by N<sub>2</sub> and CH<sub>4</sub> but enhanced by CO<sub>2</sub>. Nevertheless, the H<sub>2</sub>O surface excesses are generally two orders of magnitude lower than those of impurity gases. Therefore, the decrements of IFTs for the hydrogen-decane interface can primarily be attributed to the strong surface excesses of impurity gases according to the Gibbs adsorption equation (i.e., Eq. (10)).

### 3.4 Spreading Coefficient

The spreading coefficients of the impurity gas-H<sub>2</sub>-H<sub>2</sub>O-decane systems for different impurity gas types are given in Fig. 12. The spreading coefficients are mostly negative over the studied temperature and pressure conditions indicating the existence of three-phase contact. The spreading coefficients are larger at higher temperatures and pressures. By comparing the spreading coefficients with those from the system without impurity gases (Yang et al., 2023c), we found that the presence of impurity gases enhances the spreading coefficient and the increments are stronger at elevated temperatures and pressures. This increase of the spreading coefficient (from negative to around zero) suggests the spreading of oil lens in contact with

impurity gases.

## 4. Conclusion

We have conducted the square gradient theory calculations with PC-SAFT EoS to study the effects of the impurity gas (nitrogen, methane, and carbon dioxide) on the interfacial properties of the H<sub>2</sub>-H<sub>2</sub>O-n-C<sub>10</sub>H<sub>22</sub> three-phase systems with same mole fraction of hydrogen and impurity gas at various temperatures (298, 333, and 373 K) and pressures (up to 110 MPa). Our results in the four-component three-phase systems were compared to the corresponding system without impurity gases (Yang et al., 2023c). We found that the presence of impurity gases has a significant impact on all three interfaces (H<sub>2</sub>-H<sub>2</sub>O, H<sub>2</sub>O-C<sub>10</sub>H<sub>22</sub>, and H<sub>2</sub>-C<sub>10</sub>H<sub>22</sub>). These impurity gases accumulate in the interfacial regions and result in positive surface excesses, weakening IFT values. The extent of IFT reduction depends on the type of impurity gas, with CO<sub>2</sub> having the greatest effect, followed by CH<sub>4</sub>, and then N<sub>2</sub>. Typically, the presence of impurity gases reduces the adsorption of other substances. However, in the H<sub>2</sub>-H<sub>2</sub>O interface, the impurity gases can enhance the surface excesses of decane, contributing to the decreases in IFT. Furthermore, under the temperature and pressure conditions examined, the majority of spreading coefficients are found to be negative, indicating the presence of a three-phase contact. The presence of impurity gases enhances the spreading coefficient, and this effect is more pronounced at higher temperatures and pressures. This study contributes to the fundamental understanding of the interfacial properties of the H<sub>2</sub>-water-oil 3-phase systems in the presence of impurity gases. It could have potential applications in large-scale storage of hydrogen in depleted oil reservoirs.

## Acknowledgements

This project is supported by the National Natural Science Foundation of China (No. 42203041), the Natural Science Foundation of Jiangsu Province (No. BK20221132), and the China Postdoctoral Science Foundation (No. 2022M723398).

## Supplementary file

<https://doi.org/10.46690/capi.2023.10.02>

## Conflict of interest

The authors declare no competing interest.

## References

- Abas, N., Kalair, A., Khan, N. Review of fossil fuels and future energy technologies. *Futures*, 2015, 69: 31-49.
- Alanazi, A., Ali, M., Bawazeer, S., et al. Evaluation of cubic, PC-SAFT, and GERG2008 equations of state for accurate calculations of thermophysical properties of hydrogen-blend mixtures. *Energy Reports*, 2022, 8: 13876-13899.
- Alanazi, A., Yekeen, N., Ali, M., et al. Influence of organics and gas mixing on hydrogen/brine and methane/brine wettability using Jordanian oil shale rocks: Implications for hydrogen geological storage. *Journal of Energy Storage*, 2023, 62: 106865.
- Amin, R., Smith, T. N. Interfacial tension and spreading coef-

- ficient under reservoir conditions. *Fluid Phase Equilibria*, 1998, 142(1-2): 231-241.
- Ayirala, S. C., Xu, W., Rao, D. N. Interfacial behaviour of complex hydrocarbon fluids at elevated pressures and temperatures. *The Canadian Journal of Chemical Engineering*, 2006, 84(1): 22-32.
- Bachu, S. CO<sub>2</sub> storage in geological media: Role, means, status and barriers to deployment. *Progress in Energy and Combustion Science*, 2008, 34(2): 254-273.
- Bahramian, A., Danesh, A., Gozalpour, F., et al. Vapour-liquid interfacial tension of water and hydrocarbon mixture at high pressure and high temperature conditions. *Fluid Phase Equilibria*, 2007, 252(1-2): 66-73.
- Becker, S., Werth, S., Horsch, M., et al. Interfacial tension and adsorption in the binary system ethanol and carbon dioxide: Experiments, molecular simulation and density gradient theory. *Fluid Phase Equilibria*, 2016, 427: 476-487.
- Bertrand, E., Bonn, D., Meunier, J., et al. Wetting of alkanes on water. *Physical Review Letters*, 2001, 86(14): 3208.
- Bonn, D., Eggers, J., Indekeu, J., et al. Wetting and spreading. *Reviews of Modern Physics*, 2009, 81(2): 739.
- Chapoy, A., Mohammadi, A. H., Tohidi, B., et al. Gas solubility measurement and modeling for the nitrogen+ water system from 274.18 K to 363.02 K. *Journal of Chemical & Engineering Data*, 2004, 49(4): 1110-1115.
- Choudhary, N., Narayanan Nair, A. K., Che Ruslan, M. F. A., et al. Bulk and interfacial properties of decane in the presence of carbon dioxide, methane, and their mixture. *Scientific Reports*, 2019, 9(1): 19784.
- Chow, Y. F., Maitland, G. C., Trusler, J. M. Interfacial tensions of the (CO<sub>2</sub>+ N<sub>2</sub>+ H<sub>2</sub>O) system at temperatures of (298 to 448) K and pressures up to 40 MPa. *The Journal of Chemical Thermodynamics*, 2016, 93: 392-403.
- Chow, Y. F., Maitland, G. C., Trusler, J. M. Interfacial tensions of (H<sub>2</sub>O+ H<sub>2</sub>) and (H<sub>2</sub>O+ CO<sub>2</sub>+ H<sub>2</sub>) systems at temperatures of (298-448) K and pressures up to 45 MPa. *Fluid Phase Equilibria*, 2018, 475: 37-44.
- Chow, Y. F., Maitland, G. C., Trusler, J. M. Erratum to "Interfacial tensions of (H<sub>2</sub>O+ H<sub>2</sub>) and (H<sub>2</sub>O+ CO<sub>2</sub>+ H<sub>2</sub>) systems at temperatures of (298 to 448) K and pressures up to 45 MPa"[*Fluid Phase Equil.* 475 (2018) 37-44]., 2020, 503: 112315.
- Cornelisse, P., Peters, C., de Swaan Arons, J. Application of the Peng-Robinson equation of state to calculate interfacial tensions and profiles at vapour-liquid interfaces. *Fluid Phase Equilibria*, 1993, 82: 119-129.
- Davis, H. T. *Statistical Mechanics of Phases, Interfaces, and Thin Films*. Weinheim, Germany, Wiley-VCH, 1996.
- Davis, H. T., Scriven, L. *Stress and structure in fluid interfaces*. *Advances in Chemical Physics*, 1982, 49: 357-454.
- Diamantonis, N. I., Economou, I. G. Evaluation of statistical associating fluid theory (SAFT) and perturbed chain-SAFT equations of state for the calculation of thermodynamic derivative properties of fluids related to carbon capture and sequestration. *Energy & Fuels*, 2011, 25(7): 3334-3343.
- Doan, Q. T., Keshavarz, A., Miranda, C. R., et al. Molecular dynamics simulation of interfacial tension of the CO<sub>2</sub>-CH<sub>4</sub>-water and H<sub>2</sub>-CH<sub>4</sub>-water systems at the temperature of 300 K and 323 K and pressure up to 70 MPa. *Journal of Energy Storage*, 2023, 66: 107470.
- Florusse, L., Peters, C., Pàmies, J., et al. Solubility of hydrogen in heavy n-alkanes: Experiments and soft modeling. *AIChE Journal*, 2003, 49(12): 3260-3269
- Gbadamosi, A. O., Muhammed, N. S., Patil, S., et al. Underground hydrogen storage: A critical assessment of fluid-fluid and fluid-rock interactions. *Journal of Energy Storage*, 2023, 72: 108473.
- Georgiadis, A., Llovel, F., Bismarck, A., et al. Interfacial tension measurements and modelling of (carbon dioxide+ n-alkane) and (carbon dioxide+ water) binary mixtures at elevated pressures and temperatures. *The Journal of Supercritical Fluids*, 2010, 55(2): 743-754.
- Georgiadis, A., Maitland, G., Trusler, J. M., et al. Interfacial tension measurements of the (H<sub>2</sub>O+ n-decane+ CO<sub>2</sub>) ternary system at elevated pressures and temperatures. *Journal of Chemical & Engineering Data*, 2011, 56(12): 4900-4908.
- Gross, J., Sadowski, G. Perturbed-chain SAFT: An equation of state based on a perturbation theory for chain molecules. *Industrial & Engineering Chemistry Research*, 2001, 40(4): 1244-1260.
- Gross, J., Sadowski, G. Application of the perturbed-chain SAFT equation of state to associating systems. *Industrial & Engineering Chemistry Research*, 2002, 41(22): 5510-5515.
- Harkins, W. D., Feldman, A. Films. The spreading of liquids and the spreading coefficient. *Journal of the American Chemical Society*, 1922, 44(12): 2665-2685.
- Heinemann, N., Wilkinson, M., Adie, K., et al. Cushion gas in hydrogen storage-a costly CAPEX or a valuable resource for energy crises? *Hydrogen*, 2022, 3(4): 550-563.
- Hemmati-Sarapardeh, A., Ayatollahi, S., Zolghadr, A., et al. Experimental determination of equilibrium interfacial tension for nitrogen-crude oil during the gas injection process: The role of temperature, pressure, and composition. *Journal of Chemical & Engineering Data*, 2014, 59(11): 3461-3469.
- Hosseini, M., Fahimpour, J., Ali, M., et al. Capillary sealing efficiency analysis of caprocks: Implication for hydrogen geological storage. *Energy & Fuels*, 2022, 36(7): 4065-4075.
- Isfehiani, Z. D., Sheidaie, A., Hosseini, M., et al. Interfacial tensions of (brine+ H<sub>2</sub>+ CO<sub>2</sub>) systems at gas geo-storage conditions. *Journal of Molecular Liquids*, 2023, 374: 121279.
- Jennings Jr, H. Y., Newman, G. H. The effect of temperature and pressure on the interfacial tension of water against methane-normal decane mixtures. *Society of Petroleum Engineers Journal*, 1971, 11(2): 171-175.
- Kanaani, M., Sedaei, B., Asadian Pakfar, M. Role of cushion gas on underground hydrogen storage in depleted oil reservoirs. *Journal of Energy Storage*, 2022, 45: 103783.
- Karkevandi-Talkhooncheh, A., Rostami, A., Hemmati-Sarapardeh, A., et al. Modeling minimum miscibility

- pressure during pure and impure CO<sub>2</sub> flooding using hybrid of radial basis function neural network and evolutionary techniques. *Fuel*, 2018, 220: 270-282.
- Kashefi, K., Pereira, L. M., Chapoy, A., et al. Measurement and modelling of interfacial tension in methane/water and methane/brine systems at reservoir conditions. *Fluid Phase Equilibria*, 2016, 409: 301-311.
- Lazarus, M., van Asselt, H. Fossil fuel supply and climate policy: Exploring the road less taken. *Climatic Change*, 2018, 150(1-2): 1-13.
- Li, W., Jin, Z. Molecular dynamics simulations of natural gas-water interfacial tensions over wide range of pressures. *Fuel*, 2019, 236: 480-492.
- Linstrom, P. J., Mallard, W. G. The NIST Chemistry Web-Book: A chemical data resource on the internet. *Journal of Chemical & Engineering Data*, 2001, 46(5): 1059-1063.
- Liu, J., Wang, S., Javadpour, F., et al. Hydrogen diffusion in clay slit: Implications for the geological storage. *Energy & Fuels*, 2022, 36(14): 7651-7660.
- Luboń, K., Tarkowski, R. Influence of capillary threshold pressure and injection well location on the dynamic CO<sub>2</sub> and H<sub>2</sub> storage capacity for the deep geological structure. *International Journal of Hydrogen Energy*, 2021, 46(58): 30048-30060.
- Mairhofer, J., Gross, J. Modeling properties of the one-dimensional vapor-liquid interface: Application of classical density functional and density gradient theory. *Fluid Phase Equilibria*, 2018, 458: 243-252.
- Makimura, D., Kunieda, M., Liang, Y., et al. Application of molecular simulations to CO<sub>2</sub>-enhanced oil recovery: phase equilibria and interfacial phenomena. *SPE Journal*, 2013, 18(2): 319-330.
- Miqueu, C., Miguez, J. M., Pineiro, M. M., et al. Simultaneous application of the gradient theory and Monte Carlo molecular simulation for the investigation of methane/water interfacial properties. *The Journal of Physical Chemistry B*, 2011, 115(31): 9618-9625.
- Mirchi, V., Dejam, M., Alvarado, V. Interfacial tension and contact angle measurements for hydrogen-methane mixtures/brine/oil-wet rocks at reservoir conditions. *International Journal of Hydrogen Energy*, 2022, 47(82): 34963-34975.
- Muhammed, N. S., Haq, B., Al Shehri, D. A. Hydrogen storage in depleted gas reservoirs using nitrogen cushion gas: A contact angle and surface tension study. *International Journal of Hydrogen Energy*, 2023, in press, <https://doi.org/10.1016/j.ijhydene.2023.06.208>.
- Niaz, S., Manzoor, T., Pandith, A. H. Hydrogen storage: Materials, methods and perspectives. *Renewable and Sustainable Energy Reviews*, 2015, 50: 457-469.
- Pan, H., Connolly, M., Tchelepi, H. Multiphase equilibrium calculation framework for compositional simulation of CO<sub>2</sub> injection in low-temperature reservoirs. *Industrial & Engineering Chemistry Research*, 2019, 58(5): 2052-2070.
- Pan, Z., Trusler, J. M. Experimental and modelling study of the interfacial tension of (n-decane+ carbon dioxide+ water) in the three phase region. *Fluid Phase Equilibria*, 2023a, 568: 113760.
- Pan, Z., Trusler, J. M. Measurement and modelling of the interfacial tensions of CO<sub>2</sub>+ decane-iododecane mixtures at high pressures and temperatures. *Fluid Phase Equilibria*, 2023b, 566: 113700.
- Pan, B., Yin, X., Ju, Y., et al. Underground hydrogen storage: Influencing parameters and future outlook. *Advances in Colloid and Interface Science*, 2021, 294: 102473.
- Peng, F., Wang, R., Guo, Z., et al. Molecular dynamics simulation to estimate minimum miscibility pressure for oil with pure and impure CO<sub>2</sub>. *Journal of Physics Communications*, 2018, 2(11): 115028.
- Pereira, L. M. C., Chapoy, A., Tohidi, B., et al. Vapor-liquid and liquid-liquid interfacial tension of water and hydrocarbon systems at representative reservoir conditions: Experimental and modelling results. Paper SPE 170670 Presented at SPE Annual Technical Conference and Exhibition, Amsterdam, The Netherlands, 27-29 October 2014.
- Pereira, L. M. Interfacial tension of reservoir fluids: An integrated experimental and modelling investigation. Edinburgh, Heriot-Watt University, 2016a.
- Pereira, L. M., Chapoy, A., Burgass, R., et al. Study of the impact of high temperatures and pressures on the equilibrium densities and interfacial tension of the carbon dioxide/water system. *The Journal of Chemical Thermodynamics*, 2016b, 93: 404-415.
- Pereira, L. M., Chapoy, A., Burgass, R., et al. Measurement and modelling of high pressure density and interfacial tension of (gas+ n-alkane) binary mixtures. *The Journal of Chemical Thermodynamics*, 2016c, 97: 55-69.
- Plaat, H. *Underground Gas Storage: Why and How*. Geological Society, London, Special Publications, 2009, 313: 25-37.
- Rachford, H. H., Rice, J. Procedure for use of electronic digital computers in calculating flash vaporization hydrocarbon equilibrium. *Journal of Petroleum Technology*, 1952, 4(10): 19.
- Radke, C. Gibbs adsorption equation for planar fluid-fluid interfaces: Invariant formalism. *Advances in Colloid and Interface Science*, 2015, 222: 600-614.
- Rao, D. N., Lee, J. I. Determination of gas-oil miscibility conditions by interfacial tension measurements. *Journal of Colloid and Interface Science*, 2003, 262(2): 474-482.
- Sachs, W., Meyn, V. Pressure and temperature dependence of the surface tension in the system natural gas/water principles of investigation and the first precise experimental data for pure methane/water at 25°C up to 46.8 MPa. *Colloids and Surfaces A: Physicochemical and Engineering Aspects*, 1995, 94(2-3): 291-301.
- Schleussner, C. F., Rogelj, J., Schaeffer, M., et al. Science and policy characteristics of the Paris Agreement temperature goal. *Nature Climate Change*, 2016, 6(9): 827-835.
- Shafiee, S., Topal, E. When will fossil fuel reserves be diminished? *Energy Policy*, 2009, 37(1): 181-189.
- Shaw, D. J. *Introduction to Colloid and Surface Chemistry*. Amsterdam, Netherlands, Elsevier, 1992.

- Stegemeier, G., Pennington, B., Brauer, E., et al. Interfacial tension of the methane-normal decane system. *Society of Petroleum Engineers Journal*, 1962, 2(3): 257-260.
- Stephan, S., Cárdenas, H., Mejía, A., et al. The monotonicity behavior of density profiles at vapor-liquid interfaces of mixtures. *Fluid Phase Equilibria*, 2023, 564: 113596.
- Stephan, S., Hasse, H. Enrichment at vapour-liquid interfaces of mixtures: Establishing a link between nanoscopic and macroscopic properties. *International Reviews in Physical Chemistry*, 2020, 39(3): 319-349.
- Tarkowski, R. Underground hydrogen storage: Characteristics and prospects. *Renewable and Sustainable Energy Reviews*, 2019, 105: 86-94.
- Telo da Gama, M., Evans, R. The structure and surface tension of the liquid-vapour interface near the upper critical end point of a binary mixture of Lennard-Jones fluids: I. The two phase region. *Molecular Physics*, 1983, 48(2): 229-250.
- Tsivintzelis, I., Kontogeorgis, G. M., Michelsen, M. L., et al. Modeling phase equilibria for acid gas mixtures using the CPA equation of state. Part II: Binary mixtures with CO<sub>2</sub>. *Fluid Phase Equilibria*, 2011, 306(1): 38-56.
- Wadewitz, T., Winkelmann, J. Density functional theory: Structure and interfacial properties of binary mixtures. *Berichte der Bunsengesellschaft für physikalische Chemie*, 1996, 100(11): 1825-1832.
- Wiegand, G., Franck, E. Interfacial tension between water and non-polar fluids up to 473 K and 2800 bar. *Berichte der Bunsengesellschaft für physikalische Chemie*, 1994, 98(6): 809-817.
- Yang, Y., Che Ruslan, M. F. A., Sun, S. Study of interfacial properties of water+ methane+ oil three-phase systems by a simple molecular simulation protocol. *Journal of Molecular Liquids*, 2022, 356: 118951.
- Yang, Y., Che Ruslan, M. F. A., Zhu, W., et al. Interfacial behaviors of the H<sub>2</sub>O+ CO<sub>2</sub>+ CH<sub>4</sub>+ C<sub>10</sub>H<sub>22</sub> system in three phase equilibrium: A combined molecular dynamics simulation and density gradient theory investigation. *Journal of Molecular Liquids*, 2023a, 370: 121031.
- Yang, Y., Narayanan Nair, A. K., Che Ruslan, M. F. A., et al. Bulk and interfacial properties of the decane+ water system in the presence of methane, carbon dioxide, and their mixture. *The Journal of Physical Chemistry B*, 2020, 124(43): 9556-9569.
- Yang, Y., Narayanan Nair, A. K., Zhu, W., et al. Molecular perspectives of interfacial properties of the hydrogen+ water mixture in contact with silica or kerogen. *Journal of Molecular Liquids*, 2023b, 385: 122337.
- Yang, Y., Wan, J., Li, J., et al. Molecular modeling of interfacial properties of the hydrogen+ water+ decane mixture in three-phase equilibrium. *ArXiv preprint*, 2023c, 2307: 15356.
- Yellig, W., Metcalfe, R. Determination and prediction of CO<sub>2</sub> minimum miscibility pressures. *Journal of Petroleum Technology*, 1980, 32(1): 160-168.
- Zivar, D., Kumar, S., Foroozesh, J. Underground hydrogen storage: A comprehensive review. *International Journal of Hydrogen Energy*, 2021, 46(45): 23436-23462.